Chapter 31
Spark-Ignition Engine Fueled with Methane-Hydrogen Blends

G.M. Kosmadakis, F. Moreno, J. Arroyo, M. Muñoz, and C.D. Rakopoulos

Introduction

Apart from engine-related techniques to meet stringent imposed emissions regulations and higher efficiency over a large range of operating conditions and loads, engine researchers have focused their interest on the domain of fuel-related techniques (Rakopoulos and Giakoumis 2009). It is true that considerable attention has been paid in the development of alternative fuel sources, with emphasis on liquid bio-fuels that possess the added advantage of being renewable, such as vegetable oil, bio-diesel, ethanol, butanol, and diethyl ether (Agathou and Kyritsis 2014; Rakopoulos 2012, 2013; Wang et al. 2010). Moreover, many internal combustion engines, usually converted from commercial compression- or spark-ignition engines, have been fueled with various alternative gaseous fuels, such as the most common methane (or natural gas) and liquefied petroleum gas to the most rarely syngas and biogas, for use in power generation and transportation, showing inherently clean nature of combustion with reduced emitted pollutants (Papagiannakis and Zannis 2013; Rakopoulos and Kyritsis 2006; Rakopoulos and Michos 2009). Finally, fuel blends show some interesting features, especially when hydrogen is added to a conventional fuel for combustion enhancement, due to its very high combustion speed (Kosmadakis et al. 2012).

G.M. Kosmadakis (✉) • C.D. Rakopoulos
Internal Combustion Engines Laboratory, Thermal Engineering Department, School of Mechanical Engineering, National Technical University of Athens, 9 Heroon Polytechniou St., Zografou Campus, Athens 15780, Greece
e-mail: gkosmad@central.ntua.gr; cdrakops@central.ntua.gr

F. Moreno • J. Arroyo • M. Muñoz
Laboratory of Engines, Department of Mechanical Engineering, University of Zaragoza, C/María de Luna s/n, Zaragoza 50018, Spain
e-mail: fmoreno@unizar.es; jarroyo@unizar.es; mmunoz@unizar.es

One promising fuel blend is the methane/hydrogen one. The addition of even a small hydrogen quantity in methane increases the combustion speed, improving engine efficiency, while the fuel flammability limit is extended, allowing the use of leaner mixtures. Moreover, CO_2 and HC emissions are decreased, since the initial amount of carbon in the fuel blend is decreased (Ma et al. 2008). On the other hand, nitrogen oxides (NOx) emissions are increased, because of the higher combustion velocity and burned gas temperature, while the event of knock is likely to occur for high hydrogen percentage (Moreno et al. 2012).

Various experimental facilities have been developed for the investigation of the combustion processes of methane/hydrogen blends, and the performance of SI engines under different operating conditions and strategies (Demuynck et al. 2009; Moreno et al. 2012), as well as for the in-cylinder processes and their exhaust emissions (Akansu et al. 2007). Apart from these experimental studies, there exist many simulation works focusing mainly on the engine performance parameters (Aliramezani, et al. 2013) and to some extent to the nitric oxide (NO) emissions, using the thermal NO production path (Dimopoulos et al. 2007), widely known as the "three-equation Zeldovich mechanism".

The present study concerns the extension of the combustion model of an in-house CFD code developed by the NTUA team. This model has been initially developed for the simulation of the power cycle of hydrogen-fueled SI engines, and validated over many different conditions, including variable ignition timing, compression ratio, large range of equivalence ratios, and EGR (Kosmadakis et al. 2012; Kosmadakis and Rakopoulos 2014a, b; Rakopoulos et al. 2010a, 2011). The extension of this combustion model and of the CFD code mainly concerns the introduction of the carbon chemistry. Three more species have been added (carbon dioxide, carbon monoxide and methane), together with an appropriate laminar flame speed correlation for methane fuel, making the code capable of simulating such combustion processes.

In order to validate the CFD code, appropriate measured data are used from a two-cylinder engine. It has been decided here to focus on the variable hydrogen content, keeping all other parameters constant, whereas it is planned to conduct further investigation at other conditions as well in the future. For the validation of this model, the calculated results regarding engine performance and nitric oxide emissions are compared with the corresponding measured ones. From the analysis it is concluded that the presented combustion model manages to predict adequately the engine performance within the range of examined hydrogen content. As far as the nitric oxide exhaust emissions is concerned, the model manages to capture qualitatively correct the trend as hydrogen is increased, while in absolute values a small difference exists from the measured ones. Then, a detailed investigation of flame propagation and in-cylinder combustion is implemented, revealing the capabilities of the CFD code for detailed combustion analysis and engine research.

Experimental Facilities

The experimental facilities are briefly presented next, while further details can be found in (Moreno et al. 2012).

Engine Modifications

The experimental tests were carried out on a Lombardini LGW 523 MPI spark ignition engine, with two cylinders and total swept volume of 505 cm^3. The engine was properly modified to work with gaseous fuels containing hydrogen. These modifications are briefly mentioned next. First, an additional gaseous fuel supply circuit was mounted in parallel with the original gasoline circuit. Gas injectors are designed and manufactured by Quantum, and prevent from premature failure in dry gas applications. To favour the homogeneity of the air-fuel mixture inside the cylinder, a new gas injection port was designed and installed after the inlet manifold, where the gas injectors are fitted. Both gas injectors are fed by a gas ramp connected to the gaseous fuel supply circuit of the test rig, which is explained next. The ignition system was also modified, adding two BERU coils to ignite two NGK spark plugs with low enough thermal grade to prevent problems like pre-ignition. The original engine management system has been replaced by an AEM 30-1900U Universal Programmable Engine Management System, which controls all working parameters of the engine. The crankshaft angle at which the gaseous fuels are injected has a big influence on performance, and therefore the engine was converted to sequential injection. To this end, the installation of a cam sensor was necessary, which allowed the synchronization between the strokes of the cylinders. Moreover, the original narrow band oxygen sensor was replaced by a wide band universal exhaust gas oxygen sensor (BOSCH LSU 4.2) with better control of the fuel-air equivalence ratio, especially at lean equivalence ratios. Finally, in order to perform an analysis of the combustion behavior, a piezoelectric pressure sensor (Kistler 6053CC60) was mounted in the combustion chamber, in order to acquire and analyze the pressure inside the cylinder.

Experimental Procedures

The engine was coupled to a Tecner E315 dynamometer, which allows testing engines at constant speed or load. Data acquisition system of the test bench recorded the load, speed, temperatures, pressures and fuel and air consumptions. Pollutant emissions were measured using a Signal Instruments exhaust gas analysis installation. The measurement principles are based on non-dispersive infrared for CO and CO_2, flame detector ionization for HC, chemiluminescence for NOx and paramagnetism for O_2. The pressure inside the cylinder was measured with the

piezoelectric sensor mentioned above connected to a signal conditioning and data acquisition system from National Instruments, controlled by a specific proprietary software programmed in LabVIEW. The volumetric composition of the different gaseous fuel blends tested is presented in Table 31.1.

The engine was tested at full load and at a wide range of speeds (from 2000 to 4500 rpm), but the results selected in this study to validate the model were those corresponding to 4500 rpm. The use of hydrogen blends allows the extension of the lean operation limits of the methane (Moreno et al. 2012), so an equivalence ratio of 0.8 was selected for all cases. The ignition timing was fixed at 33° CA BTDC, in order to focus on the combustion differences due to the different blend composition. The injection timing was set to 15° CA BTDC during the intake stroke for all the fuel blends. According to engine valve timing, the injection at this moment ensures that all fuel is injected, while the inlet valve is open for all cases.

All relevant measurements have been conducted at wide-open throttle (WOT), in order to reduce the pumping losses. The main specifications of this engine are given in Table 31.2.

Table 31.1 Composition of the gaseous fuel blends tested

	H_2 composition (% by vol.)	CH_4 composition (% by vol.)
Methane	0	100
G1	10	90
G2	30	70
G3	50	50

Table 31.2 Lombardini engine main specifications

Engine model and type		Lombardini engine, two-cylinder, naturally aspirated, four stroke, water-cooled
Bore		72 mm
Stroke		62 mm
Swept volume (per cylinder)		252.5 cm^3
Connecting rod length		107 mm
Compression ratio		10.7
Valves (per cylinder)		2
Engine speed		4500 rpm
Ignition timing		33° CA BTDC
Equivalence ratio		~0.8
Number of piston rings		3
Valve timing events	Inlet valve opening	5° CA BTDC
	Inlet valve closure	59° CA ABDC
	Exhaust valve opening	57° CA BBDC
	Exhaust valve closure	7° CA ATDC

CFD Code

The firing version of the CFD code developed by the NTUA team can simulate three-dimensional curvilinear domains, using the finite volume method in a collocated grid. It has been validated in previous published works (Kosmadakis et al. 2012; Kosmadakis and Rakopoulos 2014a, b; Rakopoulos et al. 2010a, 2011), where it has been revealed that it can adequately simulate the power cycle of hydrogen-fueled spark-ignition engines. In the next subsections the extended combustion model is briefly presented, as applied in the present study and its main differences with the addition of methane fuel are discussed. A detailed presentation can be found in previous publications (Kosmadakis et al. 2012, 2013; Kosmadakis and Rakopoulos 2014a, b; Rakopoulos et al. 2010a, b, 2011).

Combustion Model

The combustion model is briefly described in this section, which has been already developed and applied in previous studies for hydrogen combustion. The main difference here is that methane fuel and carbon chemistry are added in the transport equations. Only its basic features are given, since its detailed presentation is provided in previous publications (Kosmadakis et al. 2012; Rakopoulos et al. 2010a).

For the calculation of the species reaction rates, the characteristic conversion time-scale method has been followed (Abraham et al. 1985). A characteristic time-scale (τ_c) is calculated, as the sum of the laminar conversion time (τ_l) and the turbulent mixing time (τ_t), which determines to what extent the combustible gas content of each computational cell has reached its chemical equilibrium during a specific duration (equal to the computational time step). This method is followed for the calculation of the reaction rates of all chemical species considered here, namely H_2, O_2, N_2, H_2O, H, O, N, OH, CO, CO_2, and CH_4. The reaction rates for the nitric oxide (NO) derived from three different paths (thermal NO, NNH and N_2O paths) have already been discussed in (Kosmadakis and Rakopoulos 2014a, b) and will not be repeated here. Further details concerning the calculation of the reaction rates with the use of the characteristic conversion time-scale method can be found in (Rakopoulos et al. 2010a).

The correlation for the hydrogen laminar flame speed is the one proposed by (Gerke et al. 2010), which includes stretch effects. A similar correlation for methane is used, which is proposed by (Ouimette and Seers 2009), which is derived under a wide range of pressure and temperature similar to the gas properties during spark ignition. Other correlations have been examined as well (applicable over a smaller range though), with similar results. The fuel blend laminar flame speed is calculated using a Le Chatelier rule (Rakopoulos and Michos 2009), which is a rather simple calculation method, but ensures that the most reliable correlations are

used for the two fuels (hydrogen and methane), taking into consideration stretch effects. The laminar flame speed is used to track the computational cells, in which the flame has propagated during the ignition phase through the calculation of the flame radius, assuming that the flame propagation velocity is approximately equal to the laminar flame speed during this phase. When the flame reaches a critical radius, turbulent effects become dominant and then a turbulent burning velocity (u_t) is used to track the flame. The expression used for this velocity is the one proposed by Zimont/Lipatnikov and Chomiak (Lipatnikov and Chomiak 1997; Zimont 2000), in which one calibration constant exists (constant "A"), which is appropriately tuned for each fuel blend (Rakopoulos et al. 2010a). This correlation is given in Eq. (31.1).

$$u_t = A\left(u'\right)^{3/4} u_l^{1/2} D_{T,u}^{-1/4} L_t^{1/4} + u_l \qquad (31.1)$$

where A is the calibration constant that needs to be tuned, u' the rms turbulent velocity given by $u' = \sqrt{2k/3}$, u_l the stretched laminar flame speed, $D_{T,u}$ the thermal diffusivity of the unburned mixture, and L_t the turbulent integral length scale given by $L_t = 0.37\left(u'\right)^3/\varepsilon$.

Computational Details

Some initial and boundary conditions are provided from the experimental data, such as the pressure at IVC, and the inlet air (humidity in the inlet air is neglected) and hydrogen/methane flow rates. For the rest of the required conditions, reliable estimations are used, such as the gas temperature at IVC (from 380 up to 405 K as the hydrogen content increases), wall temperature at IVC (from 440 up to 450 K as the hydrogen content increases), residual gas mass fraction (around 6–7 %), and turbulent kinetic energy at IVC (constant and equal to 55 m^2/s^2 for all cases).

The constructed computational mesh has ($40 \times 40 \times 30$) grid lines along each axis (see Fig. 31.1) and has been tested for grid independence. The addition and removal of mesh layers according to the piston movement is also used, since during compression the height of the cells decreases at the dead volume. The engine is equipped with a small bowl-in-piston, and its geometry has been extrapolated with the highest possible detail from the engine design provided by the manufacturer.

The computational time step used is equal to 1° CA, which is further decreased from the beginning of the combustion period and afterwards becoming equal to 0.4° CA. Such time step is sufficient small, since the engine speed is high and equal to 4500 rpm. Finally, the only calibration constant used in the in-house CFD code, which exists in the expression of the turbulent flame speed (no calibration factors exist in the heat transfer and crevice models), has a different value for each fuel blend, which is however in the range of 0.7 (similar with hydrogen combustion).

Fig. 31.1 Computational
grid at IVC with
$40 \times 40 \times 30$ grid lines
along the x, y, z axis. The
bowl-in-piston is depicted
at the bottom
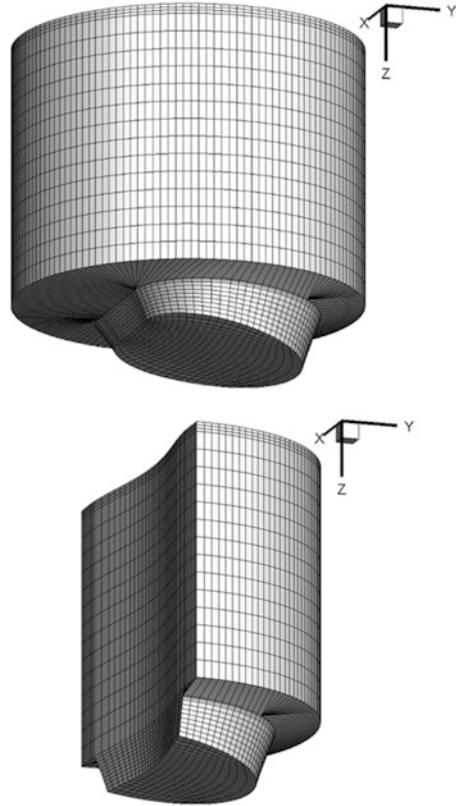
Results and Discussion

Test Cases Considered

The main engine conditions and settings of the test cases examined in the current study have been shown previously in Table 31.2. Focus is given on the effect of hydrogen content in the fuel (four test cases considered).

CFD Code Validation

The validation of the CFD code is presented here, which includes the comparison of the predicted performance and NO emissions with the available measured data for the methane/hydrogen-fueled SI engine.
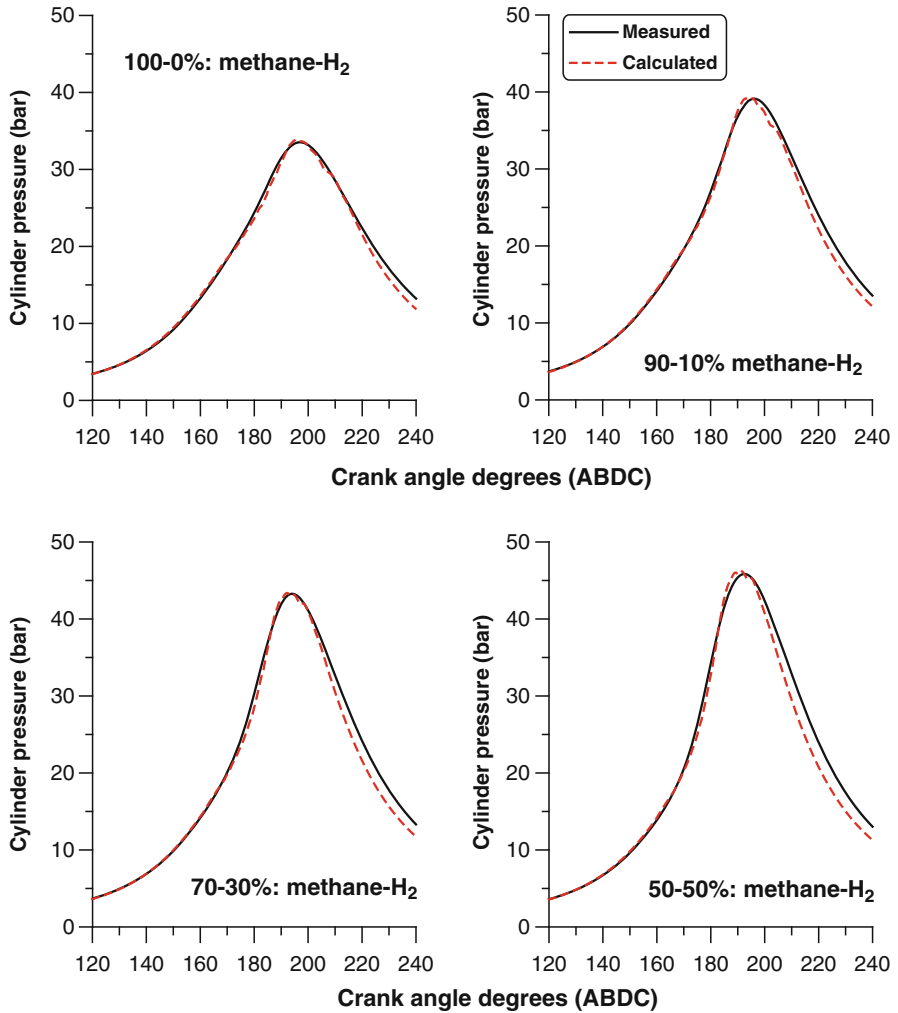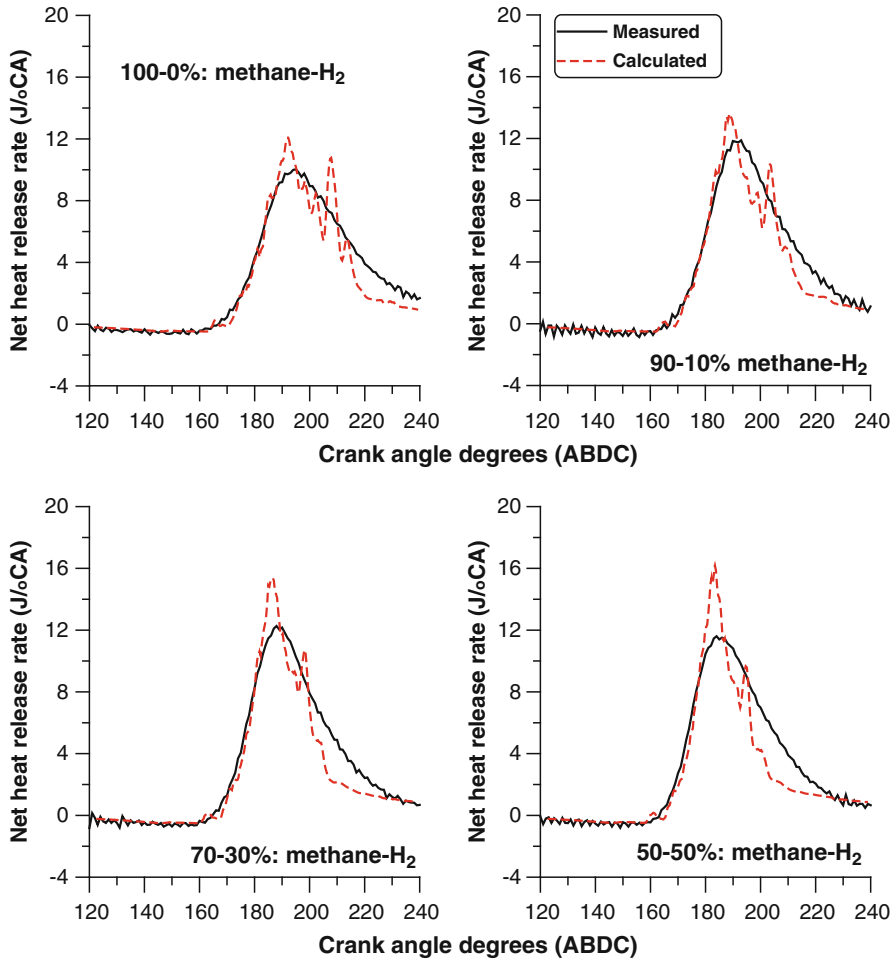
Fig. 31.2 Comparison of calculated pressure traces with the corresponding measured ones for variable hydrogen content

Engine Performance

The CFD code has been applied for the simulation of the four test cases. In Fig. 31.2 is shown the comparison of the predicted with the measured cylinder pressure for variable hydrogen content.

The pressure traces are predicted with high accuracy, since for every case considered the peak pressure and its timing are very well captured, with only some minor discrepancies. These can be partly attributed to the correlation of the laminar flame speeds used in the CFD code, being near to their application range,

Fig. 31.3 Comparison of calculated net heat release rates with the corresponding measured ones for variable hydrogen content

and to the higher heat loss calculated during the end of combustion. Nevertheless, the cylinder pressure numerical results can be considered reliable, providing a good proof of the reliability of the CFD code developed and of the presented results in the next subsections.

This conclusion is also justified with the good comparison of the net heat release rates, which is shown in Fig. 31.3. The maximum rate is well captured from the CFD code, together with the combustion timing and profile.

Again, the process during the expansion stroke shows some differences, which are under further investigation. Some possible causes can be some differences with the exact bowl geometry, a non-homogeneous gas mixture at IVC, and the uncertainty on the values of the initial gas temperature at IVC and wall temperature.

The local increase of the heat release rates during the expansion stroke at around 200° CA ABDC is due to the rapid combustion of the end gas near the cylinder liner. This is advanced as the hydrogen content is increased, due to the more rapid combustion. According to the measured values, a different trend exists, since this end gas slowly burns during a larger period at the expansion stroke.

Similar comparisons have been made concerning the indicated mean effective pressure (IMEP) and indicated efficiency. These parameters provide a more general insight on the accuracy of the numerical results using the CFD code. It has been shown that both IMEP and indicated efficiency are adequately predicted, since for all cases considered a good match exists with few differences. These exist due to the discrepancies of cylinder pressure during the exhaust stroke.

The main conclusion of this validation process is that the CFD code can predict adequately the performance of such engine with methane/hydrogen fuel blends and its application can be extended for the investigation of various conditions and engine designs.

NO Emissions

After the validation of the performance, the study focuses on the NO exhaust emissions, which are investigated for the test cases of Table 31.1. The calculated NO values are obtained using the CFD code and are compared with the measured values (see Fig. 31.4).

It can be observed that the trend of the NO emissions is adequately captured, as the hydrogen content increases. Concerning the absolute emission values there is some discrepancy, which is almost equal for all cases (around 800 ppm). For high hydrogen content, the relevant variation is maintained lower than around 30–40 %, which can be considered acceptable, since no calibration factor is included in the

Fig. 31.4 Comparison of calculated NO emissions with the corresponding measured ones for variable hydrogen content
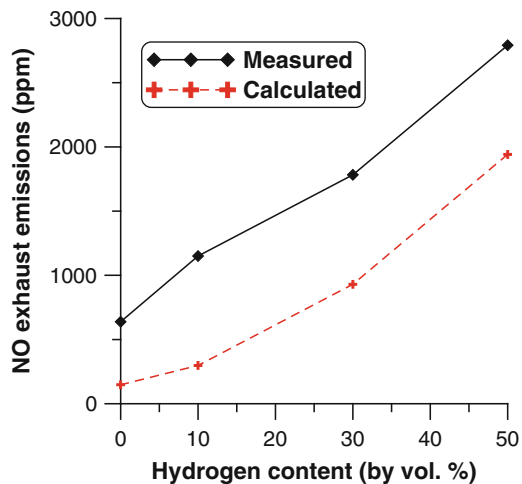
emissions model. Nevertheless, such prediction level is adequate, having in mind all uncertainty factors in the calculation of NO emissions (Kosmadakis et al. 2012; Kosmadakis and Rakopoulos 2014a).

Combustion Analysis

The validation of the extended combustion model revealed that the power cycle of a SI engine with variable hydrogen content can be simulated with detail, while both performance and NO emissions are adequately calculated. Therefore, the CFD code can be then applied for further combustion analysis, by providing some insight on the in-cylinder processes.

As the hydrogen content increases, the combustion speed is higher, increasing the gas temperatures during combustion. This is the main reason that NO emissions are higher, which is one of the main concerns for the use of hydrogen in blends (Moreno et al. 2012). Such indication is provided in Fig. 31.5, where the calculated mean gas temperature is observed. In the same figure are also shown the mean NO reaction rates, which depend a lot on the local gas temperature and the local species concentration.

It is observed that the maximum temperature (around 2400 K) is reached for the 50–50 % blend, which is observed some CA degrees before the 100–0 % blend. Also, as the hydrogen content increases, the NO reaction rates rapidly increase, since there is an exponential dependence from the temperature (Kosmadakis and Rakopoulos 2014a). Moreover, even some small addition of hydrogen in the fuel
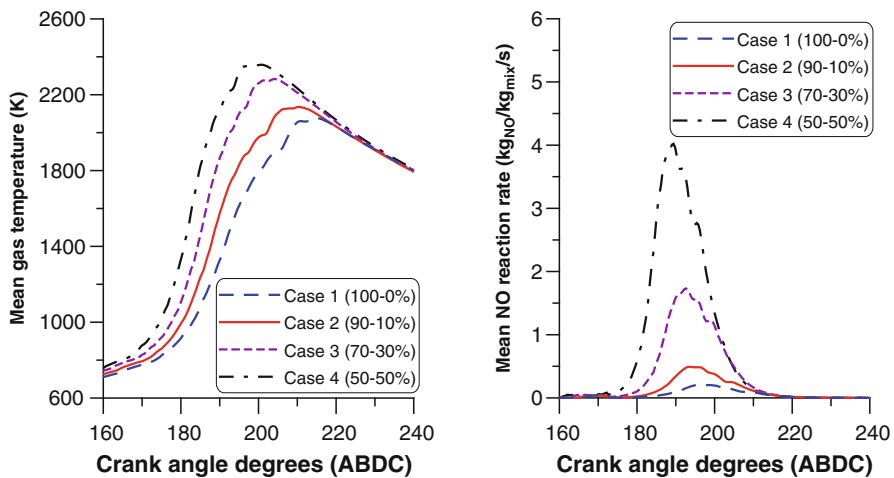
Fig. 31.5 Mean gas temperature and mean NO reaction rates during combustion and early expansion for variable hydrogen content
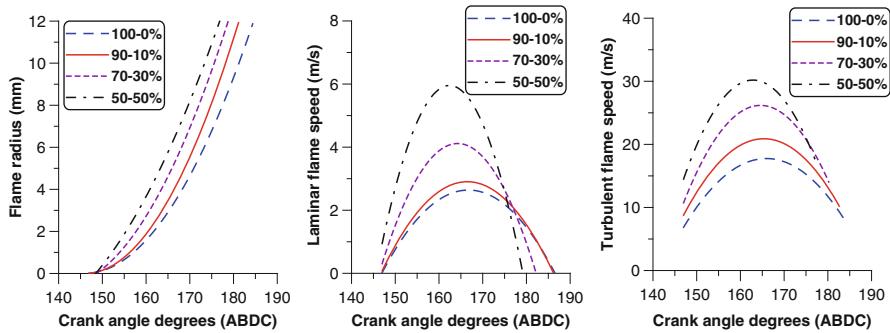
Fig. 31.6 Flame radius, laminar flame speed and turbulent flame speed for variable hydrogen content

blend, as is the case of 90–10 %, increases the maximum mean gas temperature by more than 100 K and almost doubles the mean NO reaction rate.

Some more detailed aspects of flame propagation are presented next. The differences observed are mainly due to the variable hydrogen content, since all other important parameters and conditions are exactly the same for all cases. The initial temperature and pressure at IVC show some small differences, which are however negligible and do not introduce any important changes. In Fig. 31.6 is shown the flame radius, calculated from the computational cells, which are located at an axial direction crossing the spark-plug, and until the flame reaches the piston. In the same figure is also shown the mean laminar flame speed during the early stages of combustion and the turbulent flame speed. It should be stressed that these speeds are mean values averaged over the cells that are inside the flame front and therefore should be only treated as indicative ones.

The spark-timing is constant and equal to 147° CA ABDC. Therefore, for all cases the combustion starts at the same time and it is possible to identify the effect of hydrogen addition on the flame speeds and flame propagation inside the cylinder. It is observed that the flame radius increases more quickly for higher hydrogen content, which is directly related with the mixture laminar flame speed (the hydrogen laminar flame speed is many times higher than the methane one) and turbulent flame speed. The latter mainly depends on the local turbulent properties and the laminar flame speed. These properties are more or less the same for all cases, since a constant value of turbulence has been considered for all cases (engine speed is 4500 rpm). Therefore, the turbulent flame speed depends almost exclusively on the laminar flame speed. For the 50–50 % blend, its maximum value is around twice the maximum value for the pure methane case. In other words, flame propagation is around two times higher, in case hydrogen is added in methane by 50 % by vol. This is verified by the combustion duration angles (0–5 and 5–95 %), but it can be better visualized by the flame images, shown in Fig. 31.7. These images depict how the flame propagates inside the cylinder after the ignition timing,
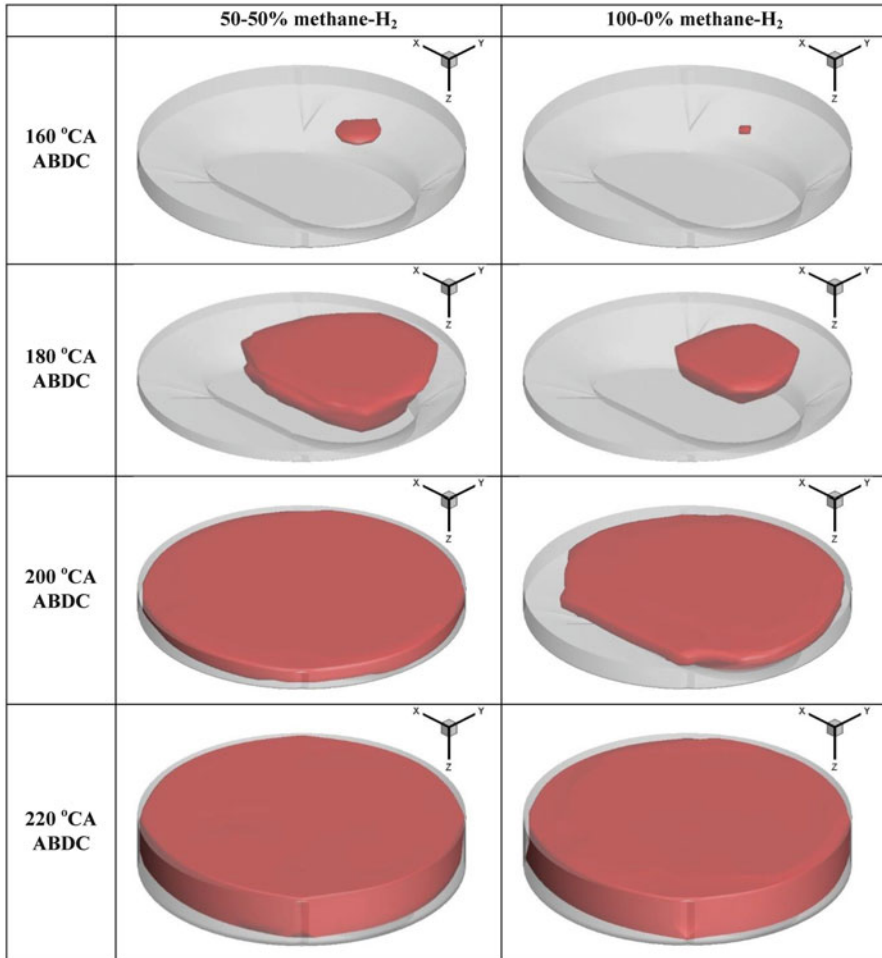
Fig. 31.7   In-cylinder flame images for 50–50 % hydrogen/methane blend and pure methane

noticing the differences for the various hydrogen contents. The spark-plug is offset from the cylinder axis, as one can guess from the location of the ignition kernel.

Owing to the high burning velocity of hydrogen, the flame has significantly expanded at TDC for the 50–50 % blend. Moreover, the flame has covered the whole combustion chamber at around 200° CA ABDC for the 50–50 % blend, and at 220° CA ABDC for the pure methane case. The main differences can be identified during early combustion, where the flame propagates with its laminar flame speed, which is much lower for the pure methane case, as mentioned previously.

Summary and Conclusions

In the present work, the combustion model of a 3D-CFD code has been extended. This was originally developed for pure hydrogen combustion, while this extension allowed it to simulate the power cycle of hydrogen/methane blends. The first step was to validate the code. Therefore, detailed measurements on a SI engine have been used for that purpose. The experimental data are for constant equivalence ratio and load, while only the hydrogen content is varied within the range 0–50 % by vol. The validation has been conducted for both performance and NO emissions. This procedure showed that the CFD code is capable of predicting the performance parameters of such engine for variable hydrogen content, while the NO emissions are adequately predicted and closely following the same trend as the measured ones. Such conclusions are encouraging, in order to apply the CFD code for further combustion analysis. Some first relevant tasks have been presented in the second part of this work, where focus has been given on the flame propagation for variable hydrogen content. It has been shown that the addition of even a small amount of hydrogen can substantially increase the flame speed, especially during the early combustion period.

In conclusion, the results obtained so far are encouraging, by showing that the simulation of SI engines fueled with hydrogen/methane blends using a detailed numerical tool, such as the one presented here, can yield reliable results, with the use of just one calibration constant per blend. However, a more extended study should be conducted in the future, covering a wider range of operating conditions (such as variable equivalence ratio and speed), to justify the validity of the model and its ability to capture combustion phenomena without adjusting the value of the calibration constant.

References

Abraham, J., Bracco, F. V., & Reitz, R. D. (1985). Comparison of computed and measured premixed charge engine combustion. *Combustion and Flame, 60*(3), 309–322.

Agathou M. S., & Kyritsis, D. C. (2014). Experimental study of steady, quasi cone-jet electrostatic sprays of bio-butanol for engine applications. *Journal of Energy Engineering 140*(3). doi: 10.1061/(ASCE)EY.1943-7897.0000141, A4014008.

Akansu, S. O., Kahraman, N., & Ceper, B. (2007). Experimental study on a spark ignition engine fuelled by methane-hydrogen mixtures. *International Journal of Hydrogen Energy, 32*(17), 4279–4284.

Aliramezani, M., Chitsaz, I., & Mozafari, A. A. (2013). Thermodynamic modeling of partially stratified charge engine characteristics for hydrogen-methane blends at ultra-lean conditions. *International Journal of Hydrogen Energy, 38*(25), 10640–10647.

Demuynck, J., Raes, N., Zuliani, M., De Paepe, M., Sierens, R., & Verhelst, S. (2009). Local heat flux measurements in a hydrogen and methane spark ignition engine with a thermopile sensor. *International Journal of Hydrogen Energy, 34*(24), 9857–9868.

Dimopoulos, P., Rechsteiner, C., Soltic, P., Laemmle, C., & Boulouchos, K. (2007). Increase of passenger car engine efficiency with low engine-out emissions using hydrogen–natural gas mixtures: A thermodynamic analysis. *International Journal of Hydrogen Energy, 32*(14), 3073–3083.

Gerke, U., Steurs, K., Rebecchi, P., & Boulouchos, K. (2010). Derivation of burning velocities of premixed hydrogen/air flames at engine-relevant conditions using a single-cylinder compression machine with optical access. *International Journal of Hydrogen Energy, 35*(6), 2566–2577.

Kosmadakis, G. M., Pariotis, E. G., & Rakopoulos, C. D. (2013). Heat transfer and crevice flow in a hydrogen-fueled spark-ignition engine: Effect on the engine performance and NO exhaust emissions. *International Journal of Hydrogen Energy, 38*(18), 7477–7489.

Kosmadakis, G. M., & Rakopoulos, C. D. (2014a). Computational fluid dynamics investigation of alternative nitric oxide emission mechanisms in a hydrogen-fueled spark-ignition engine. *International Journal of Hydrogen Energy, 39*(22), 11774–11791.

Kosmadakis, G. M., & Rakopoulos, C. D. (2014b). Computational fluid dynamics study of alternative nitric-oxide emission mechanisms in a spark-ignition engine fueled with hydrogen and operating in a wide range of exhaust gas recirculation rates for load control. *Journal of Energy Engineering* C4014008. DOI: 10.1061/(ASCE)EY.1943-7897.0000229.

Kosmadakis, G. M., Rakopoulos, C. D., Demuynck, J., De Paepe, M., & Verhelst, S. (2012). CFD modeling and experimental study of combustion and nitric oxide emissions in hydrogen-fueled spark-ignition engine operating in a very wide range of EGR rates. *International Journal of Hydrogen Energy, 37*(14), 10917–10934.

Lipatnikov, A. N., & Chomiak, J. (1997). A simple model of unsteady turbulent flame propagation. *Transactions SAE Journal of Engines 106:*2441–2452 [SAE Paper no. 972993].

Ma, F., Liu, H., Wang, Y., Li, Y., Wang, J., & Zhao, S. (2008). Combustion and emission characteristics of a port-injection HCNG engine under various ignition timings. *International Journal of Hydrogen Energy, 33*(2), 816–822.

Moreno, F., Muñoz, M., Arroyo, J., Magén, O., Monné, C., & Suelves, I. (2012). Efficiency and emissions in a vehicle spark ignition engine fueled with hydrogen and methane blends. *International Journal of Hydrogen Energy, 37*(15), 11495–11503.

Ouimette, P., & Seers, P. (2009). Numerical comparison of premixed laminar flame velocity of methane and wood syngas. *Fuel, 88*(3), 528–533.

Papagiannakis, R. G., & Zannis, T. C. (2013). Thermodynamic analysis of combustion and pollutants formation in a wood-gas spark-ignited heavy-duty engine. *International Journal of Hydrogen Energy, 38*(28), 12446–12464.

Rakopoulos, D. C. (2012). Heat release analysis of combustion in heavy-duty turbocharged diesel engine operating on blends of diesel fuel with cottonseed or sunflower oils and their bio-diesel. *Fuel, 96*, 524–534.

Rakopoulos, D. C. (2013). Combustion and emissions of cottonseed oil and its bio-diesel in blends with either n- butanol or diethyl ether in HSDI diesel engine. *Fuel, 105*, 603–613.

Rakopoulos, C. D., & Giakoumis, E. G. (2009). *Diesel engine transient operation—principles of operation and simulation analysis*. London: Springer.

Rakopoulos, C. D., Kosmadakis, G. M., Demuynck, J., De Paepe, M., & Verhelst, S. (2011). A combined experimental and numerical study of thermal processes, performance and nitric oxide emissions in a hydrogen-fueled spark-ignition engine. *International Journal of Hydrogen Energy, 36*(8), 5163–5180.

Rakopoulos, C. D., Kosmadakis, G. M., & Pariotis, E. G. (2010a). Evaluation of a combustion model for the simulation of hydrogen spark-ignition engines using a CFD code. *International Journal of Hydrogen Energy, 35*(22), 12545–12560.

Rakopoulos, C. D., Kosmadakis, G. M., & Pariotis, E. G. (2010b). Critical evaluation of current heat transfer models used in CFD in-cylinder engine simulations and establishment of a comprehensive wall-function formulation. *Applied Energy, 87*(5), 1612–1630.

Rakopoulos, C. D., & Kyritsis, D. C. (2006). Hydrogen enrichment effects on the second law analysis of natural and landfill gas combustion in engine cylinders. *International Journal of Hydrogen Energy, 31*(10), 1384–1393.

Rakopoulos, C. D., & Michos, C. N. (2009). Generation of combustion irreversibilities in a spark ignition engine under biogas-hydrogen mixtures fueling. *International Journal of Hydrogen Energy, 34*(10), 4422–4437.

Wang, S., Ji, C., & Zhang, B. (2010). Effect of hydrogen addition on combustion and emissions performance of a spark-ignited ethanol engine at idle and stoichiometric conditions. *International Journal of Hydrogen Energy, 35*(17), 9205–9213.

Zimont, V. L. (2000). Gas premixed combustion at high turbulence. Turbulent flame closure combustion model. *Experimental Thermal and Fluid Science, 21*(1–3), 179–186.